Electric control of spin states in frustrated triangular molecular magnets

J. F. Nossa [1], M. F. Islam [2], Mark R. Pederson [2], and C. M. Canali[1]

[1]*Department of Physics and Electrical Engineering, Linnaeus University, SE-39182 Kalmar, Sweden*
[2]*Department of Physics, The University of Texas at El Paso, Texas 79968, USA*

Frustrated triangular molecular magnets are a very important class of magnetic molecules since the absence of inversion symmetry allows an external electric field to couple directly with the spin chirality that characterizes their ground state. The spin-electric coupling in these molecular magnets leads to an efficient and fast method of manipulating spin states, making them an exciting candidate for quantum information processing. The efficiency of the spin-electric coupling depends on the spin-induced electric-dipole moment of the frustrated spin configurations contributing to the chiral ground state. In this paper, we report on first-principles calculations of spin-electric coupling in a {V_3} triangular magnetic molecule. We have explicitly calculated the spin-induced charge redistribution within the magnetic centers that is responsible for the spin-electric coupling. Furthermore, we have generalized the method of calculating the strength of the spin-electric coupling to calculate any triangular spin-1/2 molecule with C_3 symmetry and have applied it to calculate the coupling strength in {V_{15}} molecular magnets.

I. INTRODUCTION

One of the most exciting applications of molecular magnets in quantum technologies is that the quantum ground states of certain magnetic molecules can be used as qubits for quantum information processing [1]. Molecules offer the advantage that their properties can be tailored chemically [2,3], which is efficient and cost-effective. The ability to manipulate the spin states of a molecule by external fields is one of the central issues addressed in molecular spintronics. Traditionally, magnetic fields are used for controlling magnetic states. But the efficient manipulation of spins by an external magnetic field at the nanoscale level has significant drawbacks. The manipulation of spins in this regime has to be performed at very small spatial (approximately nanometers) and temporal (∼1 ns) scales. This requires large magnetic fields and high spatial resolution, which is very difficult to achieve.

An alternative is to apply an electric field for spin manipulation. However, since spin does not couple to the electric field directly, the electric manipulation of spins requires the presence of strong spin-orbit coupling. In a system with strong spin-orbit interaction (SOI), an electric field can modify orbitals which in turn can change the spin states, since spin states are coupled to the orbitals through the SOI. The electric control of spins through spin-orbit coupling has been studied in magnetic semiconductors since the spin-orbit coupling is stronger in such systems [4]. Multiferroic compounds are another class of systems where the spin-electric coupling is intensely investigated because of their strong magnetoelectric effects [5–7].

However, since SOI scales with the size of the system, it is very weak in molecular magnets (MMs). Thus, electric control of the spins through SOI is inefficient and hence, alternative approaches are being investigated. It has been proposed that in spin-frustrated MMs with triangular symmetry (C_3 symmetry), the electric control of spin states can be achieved via the spin chirality of the system [8–11]. The lack of inversion symmetry in these systems allows the spins to couple with an electric field to linear order. The strength of this coupling is a crucial quantity as it determines the efficiency of this mechanism in these systems. Calculation of the coupling constant by *ab initio* methods is a challenging task. Previously, we have developed a method that allows one to calculate the strength of the spin-electric coupling by *ab initio* methods and have applied it to a {Cu_3} MM [12].

A decade after theoretical prediction, the spin-electric coupling in triangular single-molecule magnets (SMMs) was eventually observed experimentally in an {Fe_3} triangular SMM [13] in the crystal phase. By employing electron paramagnetic resonance (EPR) techniques in the presence of an in-plane external static electric field, Boudalis *et al.* [13] observed that the intensity of the absorption spectrum increases with increasing in-plane static electric field, which conclusively demonstrates that the spin-1/2 chiral ground-state doublets couple to the electric field. More recently, a direct observation of the spin-electric effect in the same {Fe_3} SMM has also been reported [14]. The spin-electric coupling has also been observed in {Cu_3} [15] and {Co_3} [16] triangular complexes. The successful experimental observation of SMMs has renewed interest in this class of MMs.

The three-center systems discussed in this paper provide ideal models for isolated spin-1/2 centers and for further understanding/the role of Dzyaloshinskii-Moriya coupling [17,18] in systems lacking an inversion center. The focus of this work is on identifying structural features that can be correlated with the strength of the one-molecule spin-electric coupling, in perfectly symmetric qubits, and provide an in-depth explanation of the method for building simple model

Hamiltonians that can be quantitatively built from density functional theory (DFT) calculations. The specific study of systems with spin-1/2 centers provides a baseline theory for cases where more complex magnetocoupling arises due to the possibility of on-site localized spin excitations. Such work is needed as the basis of future model Hamiltonians that can be used to understand more complicated physics associated with an entanglement between three-fermion systems with inequivalent spins or for systems of coupled three-center qubits. Nonequilateral arrangements of spin-1/2 particles are relevant to investigations of single electrons interacting with two-center systems [19], cases where structural distortions or spin crossover break the C_3 symmetry [20,21], or systems where low-lying spin crossover may be observed on one of the metal centers. Examples of experimentally synthesized systems that may be viewed as *n*-tuples of three-center qubits include Mn$_3$ dimers [22–24].

While significant progress has been made in understanding the properties of different triangular molecular complexes since the original prediction, both theoretically and experimentally [25,26], it is not yet clear what kind of molecules have strong spin-electric coupling. To address this issue, in this work, we have investigated K$_{12}$[(VO)$_3$(BiW$_9$O$_{33}$)$_2$ · 29H$_2$O MM [27] (hereafter {V$_3$}), which is very similar to {Cu$_3$} MM except that the distance between V atoms is larger than that between Cu atoms in {Cu$_3$}. We also have studied K$_6$[V$_{15}$As$_6$O$_{42}$(H$_2$O)]8H$_2$O MM [28] (hereafter {V$_{15}$}) which, unlike {Cu$_3$} and {V$_3$}, has 15 magnetic atoms. The spin-electric coupling in triangular molecules is achieved through the chirality of the ground state of these molecules. Construction of the chiral ground states for triangular MMs such as {Cu$_3$} and {V$_3$} is rather simple as only three magnetic centers are involved. On the other hand, the construction of chiral states for the {V$_{15}$} MM requires some generalization as it involves 15 magnetic centers. Therefore, here we also present a method for constructing the chiral states of the {V$_{15}$} molecule and the calculation of spin-electric coupling in generalized chiral states.

The organization of this paper is as follows. In Sec. II we describe the mechanism of spin-electric coupling in frustrated antiferromagnetically ordered MMs with D_{3h} symmetry. In Sec. III we discuss the details of electronic structures of the {V$_3$} and {V$_{15}$} molecules we have investigated in this work, and finally in Sec. IV we discuss the results of our calculations. The estimation of different Hubbard model parameters is discussed in the Appendix.

II. SPIN-ELECTRIC COUPLING VIA CHIRAL STATES IN C_3-SYMMETRIC MMS

The lower energy regime of a spin-frustrated triangular MM is composed of two twofold degenerate chiral states. Based on a spin model and symmetry properties of the triangular molecule, one can demonstrate that electric fields can couple states of opposite chirality but with the same spin through the spin-induced dipole moment [9,11].

The strength of the spin-electric dipole coupling constant determines the effectiveness of the manipulation of the spin states by electric fields. A precise estimate of this strength
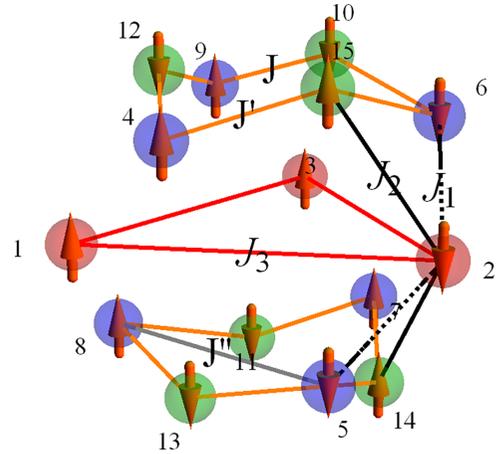

FIG. 1. Spin structure of one of the ground-state spin configurations of the {V$_{15}$} molecular magnet. There are six exchange parameters in this molecule, namely, J_1, J_2, J_3, J, J', and J''. These parameters have been calculated previously by *ab initio* methods [30]. See Fig. 7 for the full molecular structure.

constant cannot be obtained analytically and has to be determined by *ab initio* calculations or through experiments. Note that, apart from the EPR techniques mentioned above, a direct way to probe the strength of the spin-electric coupling *d* would be via Coulomb-blockade transport experiments on *individual* molecules in the cotunneling regime [29]. To date, such experiments have not been carried out yet, due to the difficulty of realizing molecular systems anchored to conducting leads, where the crucial C_3 symmetry is preserved.

In this section, we first describe the generalization of chiral states in a MM of 15 magnetic centers called {V$_{15}$} MM (see Fig. 1). We then derive an expression for the spin-electric coupling in the generalized {V$_{15}$} MM chiral states.

A. Construction of chiral ground state of {V$_{15}$} MM

Chiral states have usually been well defined for a three-site triangular MM such as {Cu$_3$} [12]. However, the unique cluster anion {V$_{15}$} [31] contains 15 V^{+4} ions ($S_i = 1/2$). It exhibits layers of different magnetization. There are two hexagon layers sandwiching a triangular central belt layer. The isotropic Heisenberg exchange Hamiltonian for the {V$_{15}$} MM can be written as

$$H_H = \sum_{\langle i,j \rangle}^{15} J_{ij} \mathbf{s}_i \cdot \mathbf{s}_j, \quad J_{ij} > 0, \tag{1}$$

where J_{ij} is the Heisenberg exchange parameter between the spins $\mathbf{s}_i$ and $\mathbf{s}_j$.

The size of the Hilbert space for this molecule is $2^{15} = 32\,768$. To obtain all the spin states of the system one needs to diagonalize the Hamiltonian in this large basis set. However, to study the spin-electric coupling in {V$_{15}$}, we need to focus only on the $S_z = 1/2$ ground-state subspace. Since total spin projection S_z of the system commutes with the Hamiltonian, we can express it in block diagonal form and work only in the $S_z = 1/2$ subspace.

By diagonalizing the Hamiltonian in the $S_z = 1/2$ subspace we obtain a twofold degenerate ground state. It contains only 1200 different spin configurations that have total spin z projection $S_z^{\text{hex}} = 0$ on the hexagonal layers of the molecule (see blue and green balls in Fig. 1). Only 1/3 of these spin configurations are associated with each of the three 1/2-spin triangular configurations at the central belt layer (see red balls labeled as 1, 2, and 3 in Fig. 1). In addition, for each of the three spin configurations of the central triangle, only 64 hexagon spin configurations are related by C_3 symmetry. These last 192 spin states contribute about 99.9% to the total $S_z = 1/2$ ground state. The two real solutions of the ground state are

$$\psi_1^R = \sum_{i=1}^{64}(a_{1i}|h_i duu\rangle + b_{1i}|h_i udu\rangle + c_{1i}|h_i uud\rangle),$$

$$\psi_2^R = \sum_{i=1}^{64}(a_{2i}|h_i duu\rangle + b_{2i}|h_i udu\rangle + c_{2i}|h_i uud\rangle), \tag{2}$$

where h_i's are different hexagon configurations for each spin arrangement of the central triangle $|duu\rangle$, $|udu\rangle$, and $|uud\rangle$. Here u and d stand for up and down spin, respectively, and a_{ji}'s and b_{ji}'s are real coefficients. The states $|h_i duu\rangle$, etc., contain information of both the orbital and the spin degrees of freedom.

To construct the chiral operator for this system we note that the exchange parameters for different pairs shown in Fig. 1 are $J = 290.3$, $J' = 222.7$, $J'' = 15.9$, $J_1 = 13.8$, $J_2 = 23.4$, and $J_3 = 0.55$ meV [30]. Clearly, the exchange interaction between the pairs in the central triangle is much weaker compared to the exchange interaction between other pairs. Therefore, the low-energy magnetic structure is determined by the three magnetic sites at the central triangle of the $\{V_{15}\}$ molecule, while the remaining 12 spins are frozen in an unfrustrated antiferromagnetic configuration with a total S_z component equal to zero. The chiral operator for this system can be defined only by these three sites as

$$C_z = \frac{4}{\sqrt{3}}\mathbf{s}_1 \cdot \mathbf{s}_2 \times \mathbf{s}_3. \tag{3}$$

Since the chiral operator, C_z, defined in Eq. (3) commutes with the spin Hamiltonian in Eq. (1), they share common eigenstates. We have obtained the chiral states by diagonalizing the chiral operator on the basis of real ground states, Eqs. (2), that gives

$$\Psi_1 = \psi_1^R + i\psi_2^R,$$
$$\Psi_2 = \psi_1^R - i\psi_2^R. \tag{4}$$

Substituting Eqs. (2) in Eqs. (4), and after some algebra, we obtain

$$\Psi_1 = \sum_{i=1}^{64} a_i(|h_i duu\rangle + \omega|h_i' udu\rangle + \omega^2|h_i'' uud\rangle),$$

$$\Psi_2 = \sum_{i=1}^{64} b_i(|h_i duu\rangle + \omega^2|h_i' udu\rangle + \omega|h_i'' uud\rangle). \tag{5}$$

Here, $\omega = e^{i2\pi/3}$ and a_i, b_i are complex coefficients. In these complex solutions of the Heisenberg model, the hexagonal
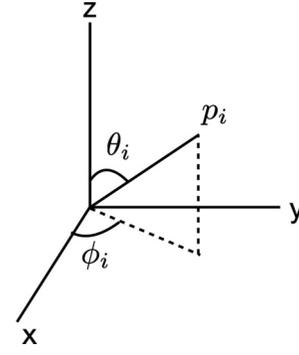

FIG. 2. Dipole moment of one of the spin configurations in Eq. (8). The absence of σ_h symmetry in $\{V_{15}\}$ allows the dipole moment to point away from the central triangular plane.

parts contributing to the three terms of the chiral GS are not the same as those appearing in the real solutions of Eqs. (2). In this case, the three terms in the sum are related by C_3 symmetry. To distinguish this case, we have labeled the hexagonal parts by h, h', h'' in Eqs. (5). Note that Ψ_1 and Ψ_2 are states of opposite chirality. An external electric field can couple these states through the induced dipole moment.

Alternatively, we can treat the effect of the chiral operator as a small perturbation and diagonalize the Hamiltonian,

$$H_{\text{H}} = \sum_{\langle i,j \rangle}^{15} J_{ij}\mathbf{s}_i \cdot \mathbf{s}_j + \lambda C_z, \quad J_{ij} > 0, \tag{6}$$

in the basis of 1200 spin configurations of $S_z = 1/2$ subspace and obtain the same chiral ground state as above.

B. Spin-electric coupling in the $\{V_{15}\}$ MM

An external electric field couples states of opposite chirality but same spin. Therefore, we are interested in calculating the matrix element

$$\langle \Psi_1 | e\vec{E} \cdot \vec{r} | \Psi_2 \rangle = e\vec{E} \cdot \langle \Psi_1 | \vec{r} | \Psi_2 \rangle = e\vec{E} \cdot \vec{d}. \tag{7}$$

Substituting Eqs. (5) in Eq. (7) and using the spin orthogonality of different basis states $|h_i duu\rangle$, etc., we obtain

$$\vec{d} = \sum_{i=1}^{64} a_i^* b_i (\langle h_i duu | \vec{r} | h_i duu \rangle + \omega \langle h_i' udu | \vec{r} | h_i' udu \rangle$$

$$+ \omega^2 \langle h_i'' uud | \vec{r} | h_i'' uud \rangle)$$

$$= \sum_{i=1}^{64} a_i^* b_i (\vec{p}_i^{\,duu} + \omega \vec{p}_i^{\,udu} + \omega^2 \vec{p}_i^{\,uud})$$

$$= \sum_{i=1}^{64} a_i^* b_i \vec{p}_i. \tag{8}$$

The magnitudes of $\vec{p}_i^{\,duu}$, $\vec{p}_i^{\,udu}$, and $\vec{p}_i^{\,uud}$ are the same because of the C_3 symmetry. Thus, we can express $\vec{p}_i$ as

(see Fig. 2)

$$
\begin{aligned}
\vec{p}_i &= p_i[\sin\theta_i\cos\phi_i\widehat{x} + \sin\theta_i\sin\phi_i\widehat{y} + \omega(\sin\theta_i\cos(\phi_i + \alpha)\widehat{x} + \sin\theta_i\sin(\phi_i + \alpha)\widehat{y}) + \omega^2(\sin\theta_i\cos(\phi_i + 2\alpha)\widehat{x} \\
&\quad + \sin\theta\sin(\phi + 2\alpha)\widehat{y})] + 3p_i\cos\theta_i\widehat{z} \\
&= p_i\sin\theta_i[\{\cos\phi_i + \omega\cos(\phi_i + \alpha) + \omega^2\cos(\phi_i + 2\alpha)\}\widehat{x} + \{\sin\phi_i + \omega\sin(\phi_i + \alpha) + \omega^2\sin(\phi_i + 2\alpha)\}\widehat{y}] \\
&\quad + 3p_i\cos\theta_i\widehat{z} \\
&= \tfrac{3}{2}p_i\sin\theta_i[\{\cos\phi_i - i\sin\phi_i\}\widehat{x} + \{\sin\phi_i + i\cos\phi_i\}\widehat{y}] + 3p_i\cos\theta_i\widehat{z} \\
&= \tfrac{3}{2}[(p_{ix} - ip_{iy})\widehat{x} + (p_{iy} + ip_{ix})\widehat{y}] + 3p_{iz}.
\end{aligned} \tag{9}
$$

Here $\alpha = 120°$ and p_{ix}, p_{iy}, and p_{iz} are the components of the dipole moment p_i. Note that the out-of-plane component does not have any ω term since it coincides with the C_3 symmetry axis. The coupling matrix element is then

$$
\begin{aligned}
e\vec{E} \cdot \vec{d} &= \frac{3}{2}e\sum_{i=1}^{64}a_i^*b_i[(p_{ix} - ip_{iy})E_x + (p_{iy} + ip_{ix})E_y] \\
&\quad + 3e\sum_{i=1}^{64}a_i^*b_ip_{iz}E_z \\
&= eE_\parallel\frac{3}{2}\sum_{i=1}^{64}a_i^*b_i[(p_{ix} - ip_{iy}) + (p_{iy} + ip_{ix})] \\
&\quad + eE_z3\sum_{i=1}^{64}a_i^*b_ip_{iz}.
\end{aligned} \tag{10}
$$

Since the electric field is an external control parameter and does not affect the strength of the coupling, we can apply it in any convenient direction. To simplify the calculations, we apply the field in a direction such that $E_x = E_y = E_\parallel$. We can split the spin-electric-coupling vector, $\vec{d}$, into two parts: The in-plane contribution $d_\parallel$ and the out-of-plane (perpendicular to the triangular plane) contribution d_z,

$$
|d_\parallel| = \frac{3}{2}\left|\sum_{i=1}^{64}a_i^*b_i[(p_{ix} + p_{iy}) + i(p_{ix} - p_{iy})]\right|, \tag{11}
$$

$$
|d_z| = 3\left|\sum_{i=1}^{64}a_i^*b_ip_{iz}\right|. \tag{12}
$$

Since the coefficients a_i and b_i are already known from the solution of the Heisenberg model, we can calculate the coupling strength by calculating the components of the dipole moment by using DFT, which we have performed in this work. It is important to note that the symmetry of the molecule determines which components of the dipole moment contribute to the spin-electric coupling. For example, in triangular molecules with D_3 symmetry, which is the case for the {V$_{15}$} SMM, both the in-plane and the out-of-plane components of the dipole can contribute to the spin-electric coupling. Therefore, in the case of the {V$_{15}$} SMM, both the in-plane ($E\parallel$) and the out-of-plane (E_z) external electric fields can be used to manipulate the chirality qubit states.

On the other hand, in triangular molecules with D_{3h} symmetry, which is the case for the {Cu$_3$} and {V$_3$} SMMs, the z component of $\vec{d}$ is zero, since the the z cannot couple the states of the opposite chirality for this symmetry. Therefore, only the $d_\parallel$ component of the dipole contributes to the electric coupling and therefore, only an $E_\parallel$ field can manipulate the chirality qubit states. For a D_{3h}-symmetric MM with three magnetic centers such as {Cu$_3$}, {V$_3$}, etc., only three spin configurations are involved and they contribute equally to the ground state. In this case Eq. (5) reduces to

$$
\begin{aligned}
\Psi_1 &= \frac{1}{\sqrt{3}}(|duu\rangle + \omega|udu\rangle + \omega^2|uud\rangle), \\
\Psi_2 &= \frac{1}{\sqrt{3}}(|duu\rangle + \omega^2|udu\rangle + \omega|uud\rangle).
\end{aligned} \tag{13}
$$

The D_{3h} symmetry constrains the dipole moment to lie in the plane containing the three magnetic centers, along the straight line joining the midpoint between the two magnetic centers in the spin-$|\uparrow\rangle$ state and the third magnetic center within the spin-$|\downarrow\rangle$ state (see Fig. 8). In this case, $a = b = \frac{1}{\sqrt{3}}$ and $p = \sqrt{p_x^2 + p_y^2}$. Then the dipole coupling in Eq. (11) reduces to that of the three-center triangular SMMs obtained in our earlier work [12],

$$
d = \frac{p}{\sqrt{2}}. \tag{14}
$$

III. DFT CALCULATIONS OF THE ELECTRONIC STRUCTURE OF TRIANGULAR MOLECULAR MAGNETS

In this work we have investigated the {V$_3$} and {V$_{15}$} MMs. Here we present the electronic structure of these molecules. Our results show that a spin model of three exchange-coupled spins $s = 1/2$ is useful to understand the magnetic properties of triangular MMs. However, all the other atoms in the molecule are essential for its geometrical stability and for the resulting superexchange interaction among the spins at the magnetic sites. Therefore, for a proper *ab initio* description of the molecule, these atoms must be included to a certain extent in the calculations.

The theoretical studies have been carried out using the NRLMOL *ab initio* package (Refs. [32,33]) that uses a Gaussian basis set to solve the Kohn-Sham equations using Perdew-Burke-Ernzerhof [34] generalized gradient approximation. All-electron calculations are performed for all elements of the molecule except for tungsten and bismuth, for which we have used pseudopotentials. Prior to geometry relaxation, an initial net total spin configuration for the triangular core was
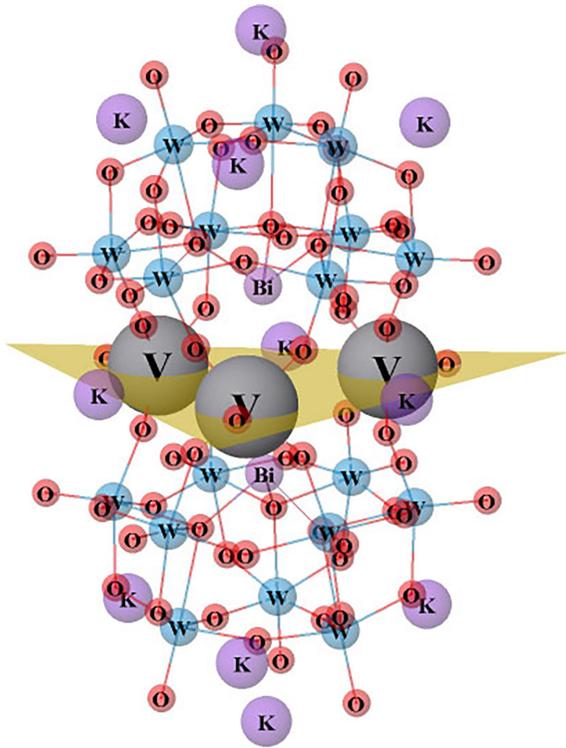
FIG. 3. Ball and stick model of the {V$_3$} molecular magnet with chemical composition K$_{12}$[(VO)$_3$(BiW$_9$O$_{33}$)$_2$] · 29H$_2$O [27].

FIG. 4. The majority (blue) and minority (red) density of d states of the {V$_3$} MM. The dotted line corresponds to the Fermi level. The inset shows the states near the Fermi level and the HOMO-LUMO gap.

assigned to $S = 3/2$. Self-consistency was reached when the total energy converged to 10^{-6} hartree or less. After optimization, the net spin was changed to $S = 1/2$ to obtain the ground-state energy.

A. {V$_3$}

The model of a {V$_3$} MM used in this calculation consists of 104 atoms. The molecule has D_{3h} symmetry with three V^{4+} ions forming an equilateral triangle as shown in Fig. 3. While the chemical composition of {V$_3$} is not exactly the same as that of the {Cu$_3$} SMM [Na$_{12}$[Cu$_3$(AsW$_9$O$_{33}$)$_2$3H$_2$O] · 32H$_2$O], the two molecules are structurally similar except that the distance between the V ions in {V$_3$} is 5.69 Å, which is larger than the separation between the Cu ions in the {Cu$_3$} MM. More importantly, their symmetry properties are identical as both MMs belong to the same point group. In this section we will focus on the electronic properties of {V$_3$} only, since the details of the electronic properties of the {Cu$_3$} MM are discussed in Ref. [12].

The three V^{4+} ions are the sites of three identical $s = 1/2$ quantum spins. The frontier electrons on each of these sites are primarily of d character. Figure 4 shows the density of states of the {V$_3$} MM where the highest occupied molecular orbital (HOMO) and the lowest unoccupied molecular orbital (LUMO) are dominated by V d electrons. The energies of the minority spin HOMO and LUMO levels are found to be −4.22 and −4.03 eV, respectively, while the majority spin HOMO and LUMO levels are found to be −4.20 and −3.96 eV, respectively. The majority-minority and minority-majority spin-flip gaps (0.17 and 0.26 eV, respectively) are
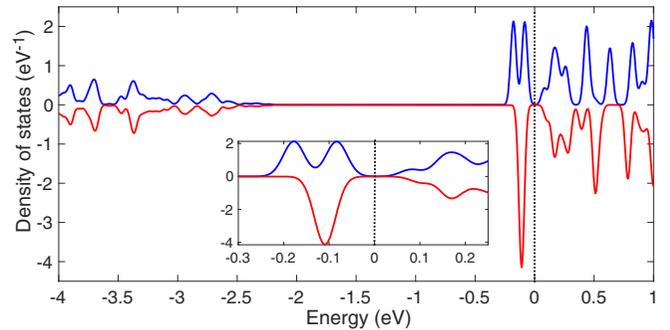
both positive, which ensures that the system is stable with respect to the total magnetic moment. The ground state of the molecule is antiferromagnetic with total spin $S = 1/2$. The exchange constant, defined as proportional to the difference between the ground $S = 1/2$ energy, E_{duu}, and the first excited $S = 3/2$ energy, E_{uuu}, is $J = 2(E_{uuu} - E_{duu})/3 \approx 1.2$ meV.

The magnetic interactions among the magnetic ions in a molecule may be of either the direct exchange or the superexchange type. Interactions mediated through the direct overlap of electronic orbitals are called direct exchange. The exchange interaction between d electrons of two V in the {V$_3$} MM is mediated either by an intermediate oxygen ion, V-O-V, or by more complicated exchange paths involving other nonmagnetic atoms such as V-O-W-O-W-O-V shown by the yellow line in Fig. 5. Superexchange interaction through two or more nonmagnetic ions is also called by some authors super-super-exchange [35]. We will, however, refer to it simply as superexchange.

Qualitative relationships for signs and values of spin-exchange interactions, for simple systems, were first developed by Goodenough [36,37], and extended by Kanamori [38]. The strengths of the superexchange interactions can be estimated in terms of the angle sustained in the V-O-V bond and the symmetry properties of the vanadium d orbitals. Superexchange involving more nonmagnetic ions, such as a V-O-W-O-W-O-V path shown in Fig. 5 (top), is far from being a trivial problem. So far there are no such qualitative rules for predicting the magnitude and sign of these interactions. In some cases, a longer-path superexchange interaction through nonmagnetic atoms can be even stronger than the direct superexchange interactions [39].

In order to understand the magnetic properties and superexchange path of the {V$_3$} MM we note that the local crystal-field symmetry of V ions is square-pyramidal as shown in Fig. 5 (bottom). The vanadyl (VO^{2+}) bond, the apex of the pyramid, is 1.59 Å, while the other, almost coplanar, V-O bonds are 1.91–1.94 Å. The d orbitals of the V ion split into different energy levels under the influence of this crystal field. In the ground state of a V^{4+} ($3d^1$) ion in a pyramidal crystal field (distorted octahedral [40]) containing a vanadyl bond, the unbounded electron is placed in the d_{xy} orbital of the t_{2g} subspace (see Fig. 6).
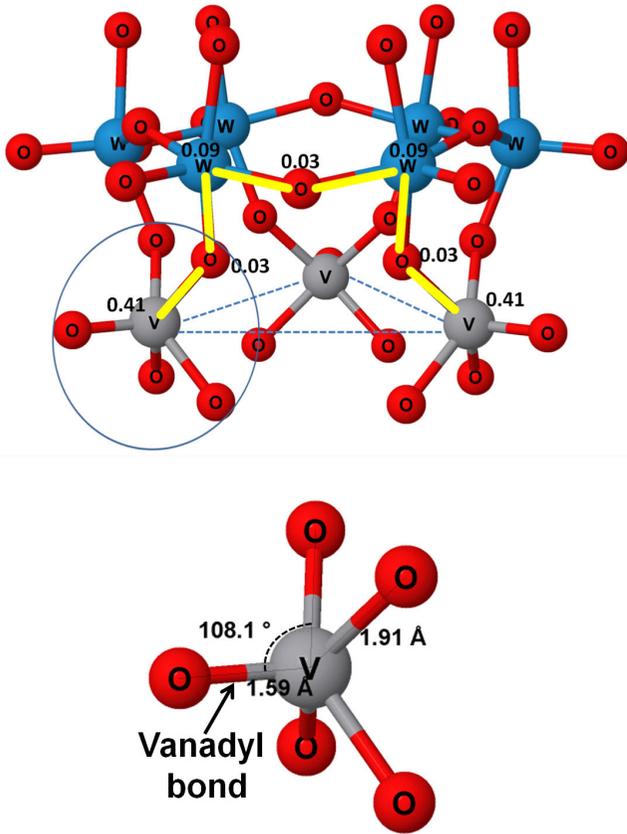
FIG. 5. Top: Superexchange coupling between two V atoms. The yellow line connecting two V atoms shows the superexchange path through three O and two W atoms. The numbers near the atoms are the magnetic moment (in units of μ_B) of the corresponding atoms along the superexchange path. Local VO$_5$ complex is marked by a blue circle. Bottom: Local square-pyramid coordination polyhedra of a V^{4+} atom.

The energy gap Δ_1 between the nondegenerate orbital d_{xy} and the first degenerate excited state, d_{yz} or d_{xz} orbitals, is much larger than $k_B T$ [41]. The spatial location of the d_{xy} orbital is perpendicular to the vanadyl bond (see Fig. 5). The
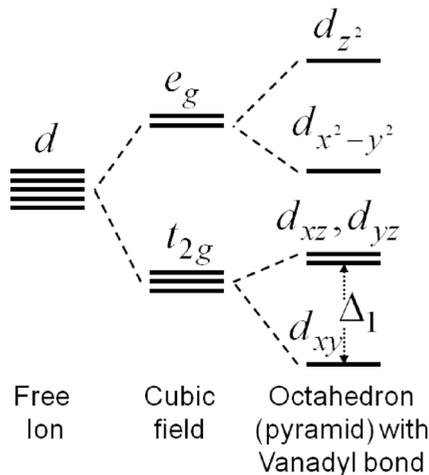

FIG. 6. Crystal-field splitting of d orbitals for the cubic field and octahedron symmetry.
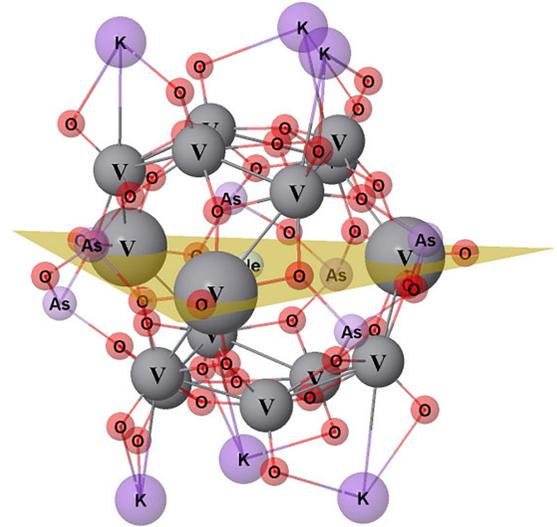

FIG. 7. Atomic configuration of the {V$_{15}$} molecular complex. Three V atoms are placed in a central triangle sandwiched by two distorted hexagons.

overlap between the d_{xy} orbitals of the V^{4+} and the surrounding equatorial p orbitals of the oxygen atoms is of π type. The d-orbital energies are shown in Fig. 6. The dominant magnetic interactions take place through these equatorial atoms while the interaction with the apical oxygen atom is expected to be much weaker.

The magnitude and sign of the resulting magnetic superexchange interaction between V^{4+} ions is much more complicated than in the case of cuprates like Cu^{2+} compounds. In the latter, the unbound electron is placed in the $d_{x^2-y^2}$ orbital, which takes part in the σ bond between copper and oxygen. Thus, the overlap and angle involved in the exchange path are clearly well defined. On the other hand, the π bond between d_{xy} of V^{4+} and surrounding oxygen ions is less well defined because its overlap strongly depends on the relative orientations between the vanadium ion and the surrounding oxygen ions.

B. V$_{15}$

The chemical composition of the {V$_{15}$} MM, synthesized by Gatteschi *et al.* [28], is K$_6$[V$_{15}$As$_6$O$_{42}$(H$_2$O)]8H$_2$O. It has 15 spins $s = 1/2$ transition metal atom V as shown in Fig. 7, which are the magnetic centers of the molecule. As shown in Fig. 7, {V$_{15}$} MM has three V atoms at the central region forming an equilateral triangle (red balls). The rest of the 12 atoms form two hexagons, one above and one below the triangle. However, the hexagons are slightly distorted. Let us consider the upper hexagon. Three of the atoms (blue upper balls) lie in a triangular plane slightly below the other three atoms of the hexagon (green upper balls). The same applies to the lower hexagon. The {V$_{15}$} MM does not have σ_h symmetry operation but the atoms in the upper hexagon are related to the corresponding atoms in the lower hexagon by the S_3 symmetry. Thus, {V$_{15}$} has D_3 symmetry.

Although {V$_{15}$} has 15 V atoms, it can be viewed as a combination of three pentanuclear subsystems. Each subsystem

TABLE I. Exchange constant J_3 between the magnetic atoms at the central triangle, dipole coupling d, distance between magnetic centers *dis*, majority HOMO-LUMO gap, and minority HOMO-LUMO gap for MMs investigated in this work.

Mol.	dist. (Å)	J_3 (meV)	d (a.u.)	Maj. HL (eV)	Min. HL (eV)
{Cu$_3$}	4.88	3.7	2.56×10^{-4}	0.72	0.69
{V$_3$}	5.70	1.3	3.56×10^{-2}	0.24	0.21
{V$_{15}$}	7.00	1	4.07×10^{-3}	1.12	1.11

consists of one V atom in the central belt and two pairs V-V from the upper and lower hexagons. For example, in Fig. 1, a subsystem consists of the balls numbered as 2, 5, 6, 14, and 15. The atoms of this pentanuclear subsystem are connected by a black line.

At low temperatures, the total magnetic moment of the ions on the hexagons is quenched due to the strong antiferromagnetic coupling between them. Thus, only the spin of the V in the central belt is active and it determines the spin of the whole subsystem. Therefore, the subsystem can be considered as an effective quasiparticle of spin $s = 1/2$ placed on the corner of a central triangle (ball number 2 for the subsystem connected by black lines). As a consequence, the entire molecule can be viewed as an effective trinuclear system of spins $s = 1/2$. [31]. This model of an effective three magnetic sites makes {V$_{15}$} a perfect candidate for spin-electric coupling just as {Cu$_3$}, and {V$_3$} MMs.

Note that although the magnetic ions on the hexagons do not contribute to the magnetic moment of the molecule, they are involved in the superexchange path between subsystems. Similarly, the construction of the chiral ground states of this molecule, which is necessary for spin-electric coupling, involves all of them (see Sec. II).

IV. RESULTS AND DISCUSSION

The *ab initio* calculations of exchange parameters and strength of spin-electric coupling for different triangular molecular magnets investigated in this work is summarized in Table I. We can note from Table I that the exchange constants of these MMs, as expected, decreases exponentially as the distance between the magnetic centers increases. A shorter superexchange path between Cu atoms in {Cu$_3$} results in the strongest exchange coupling among the molecules investigated in this work. We also note that among the molecules listed in Table I, {V$_3$} has the strongest spin-electric coupling. It is interesting to note that even with 15 magnetic centers the {V$_{15}$} MM has a weaker coupling than in {V$_3$}. The reason is that in {V$_{15}$} the dipole moments of all the spin configurations involved in the chiral ground state point along different directions, which combines to give a weaker overall coupling. Our calculations also show that in this case the strength of the in-plane and out-of-plane couplings are of the same order of magnitude.

The differences in spin-electric coupling between different molecules, as discussed in Sec. II, depend on the *spin-induced* electric dipole moments of the three spin configurations associated with $S_z = 1/2$. Their magnitudes are the same due
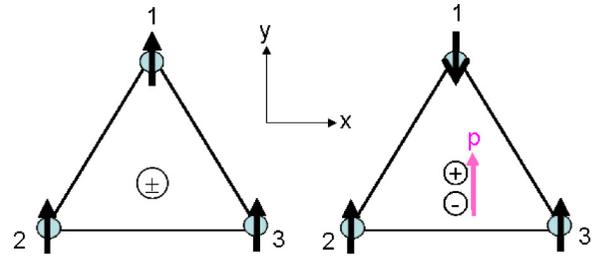

FIG. 8. Cartoon of the spin-induced dipole moment in triangular molecular magnets.

to symmetry. When the molecule is in the $S_z = 3/2$ configuration, the center of the positive and the negative charges coincide, resulting in zero dipole moment. On the other hand, if one of the spins is flipped, charges are redistributed which gives rise to a net displacement of positive and negative charge centers as shown in Fig. 8. Therefore, the average charge at a site may be different from 1.

We have carried out a calculation of the charge density of the *uuu* and *duu* spin configurations for the {Cu$_3$} and {V$_3$} molecules and then have calculated the difference in density to show the spin-induced charge transfer as shown in Fig. 9.

Our results show a charge redistribution when one spin is flipped. This leads to the appearance of a spin-induced dipole moment. In Fig. 9, blue (red) corresponds to excess (lack) of charge. From Fig. 9, we note that for the {V$_3$} MM there is a much greater concentration of blue regions at the spin-flip magnetic site compared to the {Cu$_3$} MM, where an excess of charge exists. This visible charge redistribution leads to a larger dipole moment in the {V$_3$} MM than in {Cu$_3$}. It is also interesting to notice that the color-coded charge redistribution shows the superexchange path of the molecule (see the yellow path in Figs. 5 and 9), consistent with the superexchange path specified in the experimental work on the {Cu$_3$} MM [42]. Therefore, this simple model can be used for a visual aid to obtain superexchange paths and, more importantly, to predict which molecules have stronger spin-electric coupling.

The microscopic origin of charge redistribution and the appearance of dipole moment in triangular 1/2-spin molecules can be understood from a simple one-band Hubbard model, and highlight the fact that frustrated quantum spin systems
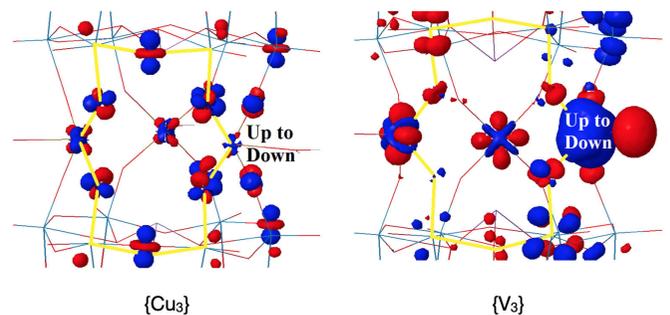

FIG. 9. Charge redistribution of the {Cu$_3$}, {V$_3$} triangular molecular magnets when one of the up spins from the *uuu* spin configuration is flipped. Blue (red) corresponds to excess (lack) of charge.

have important quantum charge fluctuations present in their ground state. As shown by Bulaevskii *et al.* [8] and Khomskii *et al.* [10,43], the charge redistribution at a magnetic site i of a triangular molecule is related to the Hubbard model parameters by

$$\delta q_i = 8\left(\frac{t}{U}\right)^3 [\mathbf{S}_i \cdot (\mathbf{S}_{i+1} + \mathbf{S}_{i+2}) - 2\mathbf{S}_{i+1} \cdot \mathbf{S}_{i+2}], \quad (15)$$

where U is on-site interaction energy, t is the hopping parameter of the Hubbard model, and $\mathbf{S}_i$ is the spin operator on-site i. The spin-induced dipole moment is given by

$$\begin{aligned} p_x &= 12ea\left(\frac{t}{U}\right)^3 \mathbf{S}_1 \cdot (\mathbf{S}_2 - \mathbf{S}_3), \\ p_y &= 4\sqrt{3}ea\left(\frac{t}{U}\right)^3 [\mathbf{S}_1 \cdot (\mathbf{S}_2 + \mathbf{S}_3) - 2\mathbf{S}_2 \cdot \mathbf{S}_3], \end{aligned} \quad (16)$$

where a is the distance between magnetic atoms in the triangle. Clearly, the charge redistribution and thus, the spin-induced dipole moment depends on the ratio, t/U. The result is consistent with the dipole coupling between two chiral states obtained by Trif *et al.* [11] and by Nossa and Canali [29].

An approximate approach to extract these Hubbard model parameters by *ab initio* methods is discussed in the Appendix. Using this approach we have calculated the parameters $U_{\{Cu_3\}} = 9.06$ eV, $t_{\{Cu_3\}} = 50$ meV, $U_{\{V_3\}} = 1$ eV, and $t_{\{V_3\}} = 53$ meV. The corresponding dipole couplings are $d_{\{Cu_3\}} = 3.48 \times 10^{-5}$ a.u. and $d_{\{V_3\}} = 3.93 \times 10^{-3}$ a.u. for the {Cu$_3$} and {V$_3$} MMs, respectively. The coupling strength obtained from Hubbard model parameters is about one order of magnitude smaller than that obtained directly from *ab initio* calculations. However, we note that the ratio of the coupling strengths is the same in both cases. The difference in the strength is probably due to the approximate nature of these calculations.

While we have not calculated the coupling strength of the {V$_{15}$} MM from the Hubbard model, our DFT calculations show that spin-electric coupling is weaker in {V$_{15}$} compared to {V$_3$}. As shown in Table I, the distance between V atoms in {V$_{15}$} is larger compared to the same atoms in {V$_3$}, resulting in weaker hopping parameter, t. Since the U parameter is not expected to be different, we can conclude from Eqs. (16) that coupling is weaker in {V$_{15}$}. However, as discussed in Sec. II, the chiral ground states of {V$_{15}$} can be also manipulated by an out-of-plane electric field. This can provide an additional advantage for the application of this SMM as a qubit since molecules are usually deposited on a surface and applying an out-of-plane electric field for such a setup may be simpler to realize.

V. SUMMARY

In this work we have calculated the spin-electric coupling strength for different triangular MMs, such as {V$_3$} and {V$_{15}$} using a first-principles method. Among these MMs, {V$_3$} has the largest spin-electric coupling constant, d. Our calculations show that the spin-electric coupling in {V$_3$} and {V$_{15}$} are two orders and one order of magnitude larger than {Cu$_3$}, respectively.

In these triangular systems, an electric field can couple states of opposite chirality but of the same spin. While the construction of chiral states in {V$_3$} is rather straightforward as only three spin configurations are involved, the construction of chiral states in {V$_{15}$} is more complicated due to 15 magnetic centers present in this MM. In this work, we have generalized the construction of chiral states for {V$_{15}$} that has D_3 symmetry. We have calculated the effect of the chiral operator on these states and have also shown how the generalized chiral states with C_3 symmetry are coupled by an external electric field. In particular, we have shown that triangular molecules lacking the σ_h mirror plane results in an out-of-plane dipole, which in turn allows an out-of-plane external electric field to couple the chiral states.

We have carried out calculations of the charge redistribution in triangular MMs. This charge redistribution occurs when one spin is flipped in an antiferromagnetic triangular MM to form a total $S = 1/2$ state. We have shown that a simple method of calculating the charge redistribution could lead to the determination of the superexchange path in such systems. This method also could be used as a fingerprint in the search for MMs with strong spin-electric coupling.

APPENDIX: HUBBARD MODEL PARAMETERS

Here we discuss the method employed to extract Hubbard model parameters from *ab initio* calculations [17].

1. Calculation of the Hubbard U

The most common approach for calculating U involves the calculation of energy, E, of the molecule with N, $N + 1$, and $N - 1$ electrons and extracting U from the equation

$$\begin{aligned} U &= E(N + 1) + E(N - 1) - 2E(N) \\ &= [E(N + 1) - E(N)] - [E(N) - E(N - 1)] \\ &= A - I. \end{aligned} \quad (A1)$$

In the above equation A is (minus) the electron affinity [44] and I is the ionization energy. For systems that are not closed shell, such as those considered here, the U value is essentially the second derivative of energy with respect to charge and
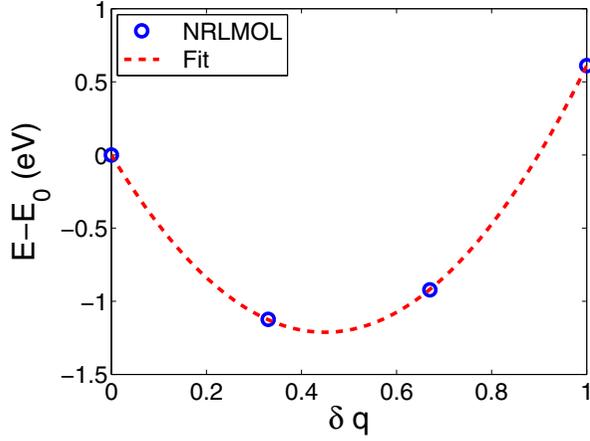
FIG. 10. Dependence of the total energy on added fractional charge δq for the $\{V_3\}$ molecular magnet. The (blue) circle represents the results of NRLMOL calculations and the dashed (red) line represents a quadratic fit.
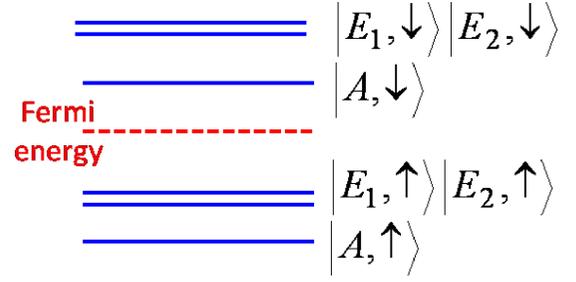

FIG. 11. Schematic diagram of the Kohn-Sham energy levels around the Fermi level.

$\delta q = 1$:

$$U_{\text{eff}} = \delta q^2 \left(\frac{\partial^2 E(q)}{\partial q^2} - \frac{e^2}{R_{\text{Cu-Cu}}} \right), \qquad \text{(A2)}$$

where $E(q) = E_0 + (U/2)(q - q_0)^2$ with E_0 being a constant.

2. Calculation of t

The Hubbard model approach is based on allowing the localized electrons to hop to its nearest-neighbor sites and in the present work these localized electrons are d electrons. Therefore, for calculating hopping parameter t, the relevant states are those d electron states that lie close to the Fermi level. Let $|K, \alpha\rangle$ be the three relevant Kohn-Sham eigenstates calculated from NRLMOL. We can write them as a linear combination of the localized atomic orbitals, centered at the three magnetic sites, $\{|\phi_a\rangle, |\phi_b\rangle, |\phi_c\rangle\} \otimes |\chi_\alpha\rangle$, with $\alpha = \uparrow, \downarrow$ for spin up and down, respectively:

$$|K, \alpha\rangle = \sum_i C_{K\alpha}^i |\phi_i\rangle |\chi_\alpha\rangle, \qquad \text{(A3)}$$

where $C_{K\alpha}^i$ is the weight of the localized $|\phi_i\rangle |\chi_\alpha\rangle$ wave function.

For the $|\uparrow \uparrow\uparrow\rangle$ spin configuration the relevant three levels around the Fermi level are doubly and singly degenerate. These levels are sketched in Fig. 11.

We obtain the level structure by diagonalizing the three-site Hamiltonian:

$$H_0 = \varepsilon_0 \sum_i |\phi_i\rangle\langle\phi_i| - t \sum_{i \neq j} |\phi_i\rangle\langle\phi_j|, \qquad \text{(A4)}$$

where ε_0 is the on-site energy, t is the hopping term, and $i, j = a, b, c$ represent the copper sites. We get the eigenvalues $\varepsilon_0 + t$ and $\varepsilon_0 - 2t$ for the twofold and onefold degenerate states, respectively. The Kohn-Sham eigenvectors can be defined as a linear combination of the localized wave functions,

$$|E_1, \uparrow\rangle = \frac{1}{\sqrt{2}}(|\phi_a\rangle - |\phi_b\rangle)|\uparrow\rangle,$$

$$|E_2, \uparrow\rangle = \frac{1}{\sqrt{6}}(|\phi_a\rangle + |\phi_b\rangle - 2|\phi_c\rangle)|\uparrow\rangle, \qquad \text{(A5)}$$

$$|A, \uparrow\rangle = \frac{1}{\sqrt{3}}(|\phi_a\rangle + |\phi_b\rangle + |\phi_c\rangle)|\uparrow\rangle.$$

it is possible to determine U by calculating the energy as a function of charge.

For the single-band Hubbard model corresponding to the molecules studied here, we are interested in obtaining energies for the charge-transfer excitations involving the transfer of a localized d electron on one ion site to a localized d electron on another site. Specifically, we wish to know the energy of $|X\rangle = |\uparrow_a \downarrow_a\uparrow_c\rangle$ relative to $|\uparrow_a \downarrow_b\uparrow_c\rangle$. There are a total of 12 charge-transfer excitations that can be made with one-site doubly occupied and one electron on one of the other sites. For the half-filled case of interest here, the energy difference depends upon the electron affinity of the state on site a, the ionization energy of the state on site b, and the residual long-range Coulomb interaction between the negatively charged electron added to site a and the positively charged hole that is left behind on site b. Since site b and site a are equivalent, it follows that we simply need to calculate U for any one of the magnetic sites in the half-filled case.

For the molecules investigated in this work, we have chosen to calculate U quasianalytically by gradually adding (or subtracting) a small fraction of electronic charge δq to one of the half-filled magnetic d states. The energy of the $\{V_3\}$ molecular magnet as a function of δq is shown in Fig. 10. We can see that it can be well reproduced by a quadratic fitting curve. The figure shows that, upon adding a fractional charge to a localized orbital, the total energy initially decreases, since the orbital energy is negative. Eventually, however, the competing Coulomb repulsion takes over and the net change in total energy for adding one electron to a localized orbital is positive. In contrast, with one extra electron delocalized throughout the molecule, the total energy is usually smaller than the energy of the neutral molecule.

The difference in the energy of the system before and after adding a fraction of electronic charge δq is given by $\Delta E = U_{\text{eff}} = U\delta q^2 - e^2\delta q^2/R_{\text{Cu-Cu}}$, where $U = \partial^2 E(q)/\partial q^2$. We have calculated the effective parameter U_{eff} by setting

Now the localized states can be written in terms of the Kohn-Sham functions

$$|\phi_a\rangle|\uparrow\rangle = \frac{|A,\uparrow\rangle}{\sqrt{3}} + \frac{|E_1,\uparrow\rangle}{\sqrt{2}} + \frac{|E_2,\uparrow\rangle}{\sqrt{6}},$$

$$|\phi_b\rangle|\uparrow\rangle = \frac{|A,\uparrow\rangle}{\sqrt{3}} - \frac{|E_1,\uparrow\rangle}{\sqrt{2}} + \frac{|E_2,\uparrow\rangle}{\sqrt{6}}, \quad \text{(A6)}$$

$$|\phi_c\rangle|\uparrow\rangle = \frac{|A,\uparrow\rangle}{\sqrt{3}} - 2\frac{|E_2,\uparrow\rangle}{\sqrt{6}}.$$

Our calculations showed that these states are primarily localized on the V and Cu atoms and have d character. We have obtained the Kohn-Sham eigenenergies for the onefold and twofold degenerate states

$$\langle E_1,\uparrow|H_0|E_1,\uparrow\rangle = \tfrac{1}{2}(\langle\phi_a| - \langle\phi_b|)H_0(|\phi_a\rangle - |\phi_b\rangle)$$

$$= \varepsilon_0 + t,$$

$$\langle A,\uparrow|H_0|A,\uparrow\rangle = \tfrac{1}{3}(\langle\phi_a| + \langle\phi_b| + \langle\phi_c|)H_0$$

$$(|\phi_a\rangle + |\phi_b\rangle + |\phi_c\rangle)) = \varepsilon_0 - 2t. \quad \text{(A7)}$$

From Eqs. (A7) we can finally evaluate the value of the parameter t as

$$t = \tfrac{1}{3}(\langle E_1,\uparrow|H_0|E_1,\uparrow\rangle - \langle A,\uparrow|H_0|A,\uparrow\rangle). \quad \text{(A8)}$$

[1] M. N. Leuenberger and D. Loss, Nature (London) **410**, 789 (2001).

[2] E. Moreno-Pineda, C. Godfrin, F. Balestro, W. Wernsdorfer, and M. Ruben, Chem. Soc. Rev. **47**, 501 (2018).

[3] M. Atzori and R. Sessoli, J. Am. Chem. Soc. **141**, 11339 (2019).

[4] D. Chiba, M. Sawicki, Y. Nishitani, Y. Nakatani, F. Matsukura, and H. Ohno, Nature (London) **455**, 515 (2008).

[5] W. Kleemann, Physics **2**, 105 (2009).

[6] D. Lebeugle, A. Mougin, M. Viret, D. Colson, and L. Ranno, Phys. Rev. Lett. **103**, 257601 (2009).

[7] K. T. Delaney, M. Mostovoy, and N. A. Spaldin, Phys. Rev. Lett. **102**, 157203 (2009).

[8] L. N. Bulaevskii, C. D. Batista, M. V. Mostovoy, and D. I. Khomskii, Phys. Rev. B **78**, 024402 (2008).

[9] M. Trif, F. Troiani, D. Stepanenko, and D. Loss, Phys. Rev. Lett. **101**, 217201 (2008).

[10] D. I. Khomskii, J. Phys.: Condens. Matter **22**, 164209 (2010).

[11] M. Trif, F. Troiani, D. Stepanenko, and D. Loss, Phys. Rev. B **82**, 045429 (2010).

[12] M. F. Islam, J. F. Nossa, C. M. Canali, and M. Pederson, Phys. Rev. B **82**, 155446 (2010).

[13] A. K. Boudalis, J. Robert, and P. Turek, Chem. Eur. J. **24**, 14896 (2018).

[14] M. Lewkowitz, J. Adams, N. S. Sullivan, P. Wang, M. Shatruk, V. Zapf, and A. S. Arvij, Sci. Rep. **13**, 2769 (2023).

[15] J. Liu, J. Mrozek, W. K. Myers, G. A. Timco, R. E. P. Winpenny, B. Kintzel, W. Plass, and A. Ardavan, Phys. Rev. Lett. **122**, 037202 (2019).

[16] B. Kintzel, M. Fittipaldi, M. Böhme, A. Cini, L. Tesi, A. Buchholz, R. Sessoli, and W. Plass, Angew. Chem., Int. Ed. **60**, 8832 (2021).

[17] J. F. Nossa, M. F. Islam, C. M. Canali, and M. R. Pederson, Phys. Rev. B **85**, 085427 (2012).

[18] J.-X. Yu, J. Chen, N. Sullivan, and H.-P. Cheng, Phys. Rev. B **106**, 054412 (2022).

[19] E. D. Switzer, X.-G. Zhang, and T. S. Rahman, J. Phys. Commun. **6**, 075007 (2022).

[20] J.-X. Yu, D.-T. Chen, J. Gu, J. Chen, J. Jiang, L. Zhang, Y. Yu, X.-G. Zhang, V. S. Zapf, and H.-P. Cheng, Phys. Rev. Lett. **124**, 227201 (2020).

[21] Z. Hooshmand and M. R. Pederson, Phys. Chem. Chem. Phys. **22**, 27547 (2020).

[22] J.-X. Yu, G. Christou, and H.-P. Cheng, J. Phys. Chem. C **124**, 14768 (2020).

[23] R. S. Berkley, Z. Hooshmand, T. Jiang, D. Le, A. F. Hebard, and T. S. Rahman, J. Phys. Chem. C **124**, 28186 (2020).

[24] T. Ghosh, J. Marbey, W. Wernsdorfer, S. Hill, K. A. Abboud, and G. Christou, Phys. Chem. Chem. Phys. **23**, 8854 (2021).

[25] B. Kintzel, M. Böhme, J. Liu, A. Burkhardt, J. Mrozek, A. Buchholz, A. Ardavan, and W. Plass, Chem. Commun. **54**, 12934 (2018).

[26] A. I. Johnson, M. F. Islam, C. M. Canali, and M. R. Pederson, J. Chem. Phys. **151**, 174105 (2019).

[27] T. Yamase, E. Ishikawa, K. Fukaya, H. Nojiri, T. Taniguchi, and T. Atake, Inorg. Chem. **43**, 8150 (2004).

[28] D. Gatteschi, L. Pardi, A. L. Barra, A. Muller, and J. Doring, Nature (London) **354**, 463 (1991).

[29] J. F. Nossa and C. M. Canali, Phys. Rev. B **89**, 235435 (2014).

[30] J. Kortus, C. S. Hellberg, and M. R. Pederson, Phys. Rev. Lett. **86**, 3400 (2001).

[31] R. Winpenny, *Molecular Cluster Magnets* (World Scientific, Singapore, 2012).

[32] M. R. Pederson and K. A. Jackson, Phys. Rev. B **41**, 7453 (1990).

[33] K. Jackson and M. R. Pederson, Phys. Rev. B **42**, 3276 (1990).

[34] J. P. Perdew, K. Burke, and M. Ernzerhof, Phys. Rev. Lett. **77**, 3865 (1996).

[35] M.-H. Whangbo, H.-J. Koo, and D. Dai, J. Solid State Chem. **176**, 417 (2003), special issue on The Impact of Theoretical Methods on Solid-State Chemistry.

[36] J. B. Goodenough, Phys. Rev. **100**, 564 (1955).

[37] J. B. Goodenough, J. Phys. Chem. Solids **6**, 287 (1958).

[38] J. Kanamori, J. Phys. Chem. Solids **10**, 87 (1959).

[39] H.-J. Koo, M.-H. Whangbo, P. D. VerNooy, C. C. Torardi, and W. J. Marshall, Inorg. Chem. **41**, 4664 (2002).

[40] M. Schindler, F. C. Hawthorne, and W. H. Baur, Chem. Mater. **12**, 1248 (2000).

[41] C. J. Ballhausen and H. B. Gray, Inorg. Chem. **1**, 111 (1962).

[42] K.-Y. Choi, Y. H. Matsuda, H. Nojiri, U. Kortz, F. Hussain, A. C. Stowe, C. Ramsey, and N. S. Dalal, Phys. Rev. Lett. **96**, 107202 (2006).

[43] D. I. Khomskii, Nat. Commun. **3**, 904 (2012).

[44] Note that usually, the electron affinity is defined as $[E(N) - E(N+1)]$, where $E(N)]$ is the energy of the neutral system.